Annealing and rejuvenation in a two-dimensional model amorphous solid under oscillatory shear

Eden Schinasi-Lemberg and Ido Regev*

The Jacob Blaustein Institutes for Desert Research, Ben-Gurion University of the Negev, Sede Boqer Campus 84990, Israel

(Received 8 September 2019; published 14 January 2020)

We study the annealing and rejuvenation behavior of a two-dimensional amorphous solid model under oscillatory shear. We show that, depending on the cooling protocol used to create the initial configuration, the mean potential energy can either decrease or increase under subyield oscillatory shear. For post-yield oscillatory shear, the mean potential energy increases and is independent on the initial conditions. We explain this behavior by modeling the dynamics using a simple model of forced dynamics on a random energy landscape and show that the model reproduces the qualitative behavior of the mean potential energy and mean-square displacement observed in the particle based simulations. This suggests that some important aspects of the dynamics of amorphous solids can be understood by studying the properties of random energy landscapes and without explicitly taking into account the complex real-space interactions which are involved in plastic deformation.

DOI: 10.1103/PhysRevE.101.012603

I. INTRODUCTION

Amorphous solids and glasses exhibit structural characteristics that are similar to liquids while responding elastically to shear forces. An amorphous solid is typically created by fast cooling a liquid into a supercooled state in which the viscosity increases rapidly and the dynamics becomes sluggish while the system avoids crystallization [1,2]. At the glass transition temperature the viscosity is so large that the effective response of the material in experimental time frames becomes that of a solid rather than a liquid (i.e., in these time scales it seems as if the viscosity is infinite) [1–3]. In the supercooled state the dynamics becomes activated and the system stays most of the time close to the minima of the potential energy function. In geometric terms, one can think of this kind of dynamics as motion on an energy surface since the potential energy,

$$u(\mathbf{r}_1, \mathbf{r}_2, ..., \mathbf{r}_N) = \sum_{i \neq j} u_{i,j}(\mathbf{r}_i, \mathbf{r}_j), \tag{1}$$

is a scalar function of the multidimensional space of configurations and thus forms a hyper-surface in this space (here $u_{i,j}$ is the energy due to a two-body interaction and $\mathbf{r}_i$ is the position of the ith particle). This energy surface is often referred to as the "energy landscape" [4] since it typically includes many different "hills" (maxima), "valleys" (minima), and saddles [5]. The energy landscape also controls the manner in which the material deforms under athermal conditions—at zero temperature the system is always at a minimum of the potential energy and when a small amount of mechanical deformation is applied, the energy landscape changes its shape and the position of the minimum shifts. When a large enough mechanical deformation is applied, the minimum merges with a close-by saddle in a saddle-node bifurcation which leads the system to "flow" to a new minimum [5,6].

In recent particle simulations and experiments, it was shown that when subject to quasi-static oscillatory shear under athermal conditions, after a transient period, an amorphous solid reaches a steady state which is either periodic, for small strain amplitudes, or chaotic/diffusive, for large strain amplitudes [7–19]. For small strain amplitudes, the steady-state potential energy was found to depend on the quenching protocol [13] while for large strain amplitudes, the steady-state potential energy was independent of the initial conditions indicating a regaining of ergodicity. This transition from asymptotically periodic to asymptotically diffusive behavior is called "the irreversibility transition" and it was found to occur at a well-defined maximal shearing amplitude γ_c. In some of these studies, that used the three-dimensional Kob-Andersen 20:80 model [20,21] and in which the initial configuration was prepared by an infinite quench from a liquid, it was found that for maximal strain amplitudes $\gamma_{\max}$ that are below the critical value, the oscillatory shear causes the zero-strain potential energy to become lower at the steady state and thus to anneal the amorphous solid. Furthermore, as long as the maximal strain amplitude is smaller than the critical value, increasing $\gamma_{\max}$ causes a decrease in the steady-state potential energy. For maximal strain amplitudes larger than the critical amplitude the steady-state potential energy increased as a function of $\gamma_{\max}$.

Since it is known that when sheared at a constant rate and direction, a glassy system can either anneal (decrease in energy) or rejuvenate (increase in energy) [22,23] a question arises as to whether this behavior can also be reproduced under oscillatory shear. One can imagine that for a system trapped inside a low energy minimum, an oscillatory forcing may cause it to escape this minimum and become trapped in a local minimum with a larger energy. Here we demonstrate such a behavior, using a two-dimensional particle model subject to athermal oscillatory shear, where the initial solid was prepared by slow cooling rather than by an infinite quench. We provide a qualitative explanation for our results using a simple model of random dynamics on a random energy landscape

*regevid@bgu.ac.il

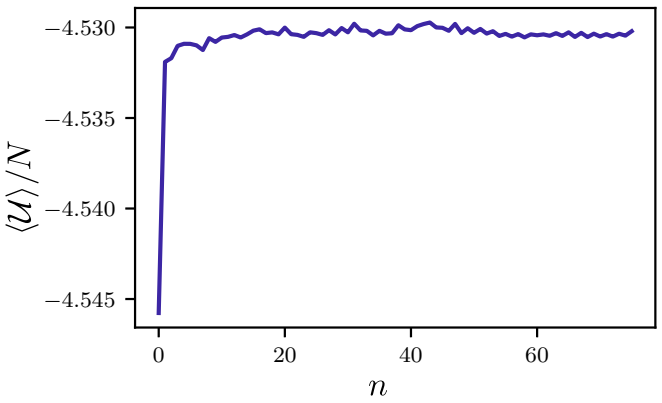

FIG. 1. Ensemble-averaged potential energy per particle at zero strain for a particle simulations with oscillatory shear with a maximal strain amplitude $\gamma_{\max} = 0.095$ as a function of the number of cycles n for initial configurations prepared by a slow quench.

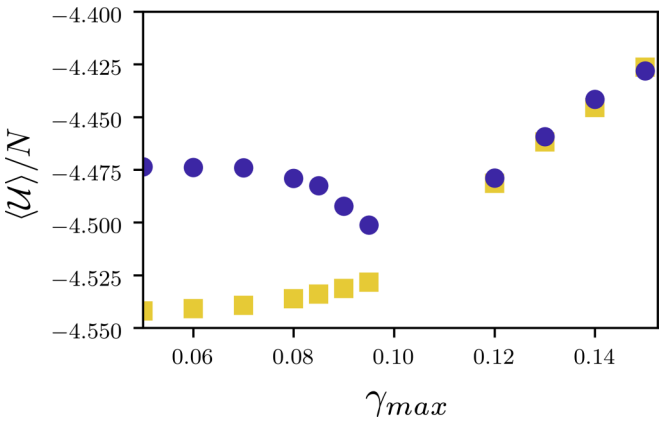

FIG. 2. Mean potential energy per particle in particle simulations ($N = 16\,384$ particles) of an amorphous solid under oscillatory shear in a-thermal quasistatic (AQS) conditions ensemble-averaged over 30 realizations. $\gamma_{\max}$ is the maximal strain amplitude and the average potential energy $\langle U \rangle$ is calculated at the steady state at zero strain. Blue dots are the steady-state energies of simulations starting from a sample prepared by a fast quench, while the yellow squares are the steady-state energies of simulations starting from a slow quench. A noticeable feature is that while the energy starting from a slow quench is always increasing, the energy starting from a fast quench is initially decreasing and starts to increase only for maximal strain amplitudes above the critical point (in this system and system size $\gamma_c \approx 0.11$).

that takes into account the features of the forcing in the particle simulations and show that it reproduces qualitatively the behavior of the steady-state potential energy and provides a simple explanation for this behavior.

II. ANNEALING AND REJUVENATION IN A MODEL GLASS

We performed simulations of a binary (50:50) mixture of $N = 16\,384$ particles interacting by a radially symmetric potential in two dimensions (see details in the Appendix). Half of the particles are 1.4 the size of the other half such that the system forms a glass due to geometrical frustration, even for relatively slow quenches. For this system and configuration, it was shown that there is an irreversibility transition at $\gamma_c \approx 0.11$ [7,8,24] (for smaller systems sizes γ_c was larger). We prepared amorphous configuration by first performing molecular dynamics simulations at a high temperature then gradually cooling the systems to a low temperature and eventually quenching the final configurations to zero temperature using a minimization algorithm. We prepared two different types of initial configurations—one type was prepared by a fast quench, while the other was prepared by a slow quench (see Appendix for details). Next, we started shearing the configurations using the usual quasi-static protocol, where the system is subject to a small strain step of magnitude $\delta\gamma = 10^{-4}$ followed by an energy minimization using the FIRE algorithm [25], and this is repeated up to a maximal strain amplitude at which the strain direction is reversed. This process is repeated periodically using a triangular progression protocol [7,13]:

$$0 \to \gamma_{\max} \to 0 \to -\gamma_{\max} \to 0 \to \ldots \tag{2}$$

with $\gamma_{\max}$ serving as a control parameter. In Fig. 1 we can see the potential energy per particle at zero strain (stroboscopic) averaged over 30 realizations for the periodic shearing with $\gamma_{\max} = 0.095$ applied to the configurations that were prepared by a slow quench. In Fig. 2 we show the steady-state potential energy for initial configurations prepared using fast (blue disks) and slow (yellow squares) quenches as a function of $\gamma_{\max}$. While the behavior for a system that was prepared by a fast quench is consistent with the annealing behavior reported for the Kob-Andersen model [20,21], we observe that for slow quenches, the potential energy increases before reaching the steady-state value and its steady-state value increases as a function of the maximal shearing amplitude $\gamma_{\max}$ even for values smaller than the critical amplitude γ_c. To explain the observed dependence of the potential energy on the applied forcing and initial configuration, we introduce a simple model for dynamics on a rough energy landscape.

III. MODEL FOR ENERGY-LANDSCAPE EXPLORATION

In the following we show that the observed behavior of the potential energy can be rationalized in terms of dynamics on an energy landscape. For this purpose we use a simple model of energy landscape dynamics which takes into account the randomness of the dynamics and the energy landscape and the effect of the external forcing. A natural question to ask is whether the dynamics under oscillatory, athermal quasistatic shear is indeed random. In particle simulations [24], it was observed that the vector of particle positions (with origin at one of the simulation box corners) moves stochastically from its initial position after a shearing cycle, as long as the system does not enter a limit cycle [Fig. 3(a)]. To demonstrate this stochasticity, we calculated the angle of the change of direction of the vector of displacements. If the vector of coordinates of the particles in the simulation after n shearing cycles is $\mathbf{r}_n = (x_1, y_1, x_2, y_2, \ldots, x_N, y_N)$, then the displacement after the $n + 1$ cycle is defined as

$$\Delta\mathbf{r}_{n+1} = \mathbf{r}_{n+1} - \mathbf{r}_n. \tag{3}$$

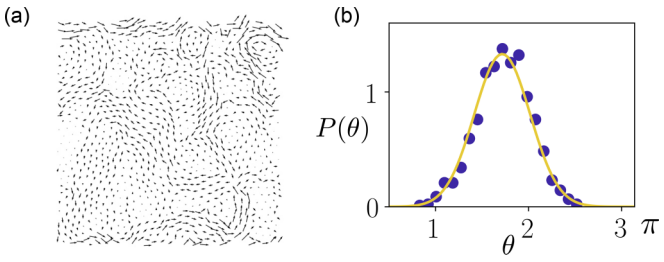

FIG. 3. (a) Displacement field after a shearing cycle of amplitude $\gamma_{\max} = 0.2$ exhibiting disordered motion. (b) A histogram of the angles between the displacement vectors after successive cycles for $\gamma_{\max} = 0.14$ showing that the angle is a random variable with an approximately Gaussian statistics (yellow line).

Using this definition, we can extract the angle between the displacements in two consecutive cycles from the scalar product:

$$\cos\theta_{n+1} = \frac{\Delta\mathbf{r}_{n+1} \cdot \Delta\mathbf{r}_n}{|\Delta\mathbf{r}_{n+1}||\Delta\mathbf{r}_n|}. \tag{4}$$

In previous work [24], we have found that the angle θ_{n+1} is random and its distribution is well-described by a normal distribution [see also Fig. 3(b)]. The randomness of the displacement is a result of the plastic events and nonaffine displacements that occur during a cycle and cause the vector of coordinates to move to a random position after each cycle.

While there is a random component to the dynamics, it is not completely random and is limited by the relation between the energy landscape surrounding the current configuration of the system and the maximal magnitude of the forcing. This is illustrated in Fig. 4 where it is shown that the effect of

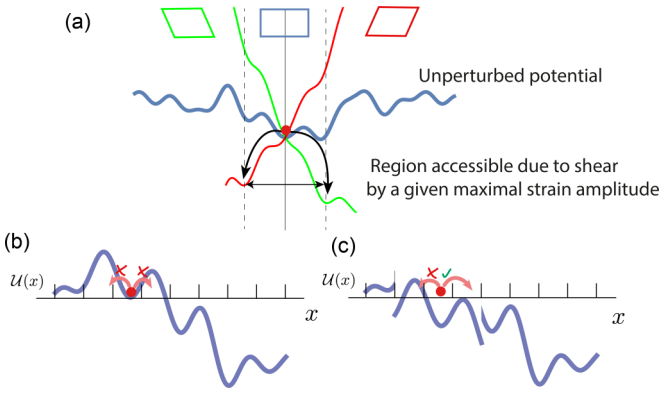

FIG. 4. (a) When shear is applied to the system it causes the energy barriers around a given minimum to decrease by a certain amount. If this decrease is large enough, then the system flows to a neighboring minimum. The exact minimum to which the system will flow depends on the barriers that are being suppressed but the motion also has a random component since typically there are many smaller minima, distributed at random, which the system traverses before it reaches the final minima (see Fig. 3). (b) To model the barrier suppression due to the forcing we lower the energy of sites surrounding the instantaneous position of the system by an external force. (c) This effectively "opens" new sites near the current position so that the system can now move to these sites (in the image the "opened" site is to the right).

applying positive and negative forcing on a random energy landscape is to "flatten" nearby energy barriers and "open" new areas for the system to explore (in the illustration—the minima to the left and right of the minimum at the current position). It is also clear from this illustration that the extent to which a forcing of a given maximal amplitude can allow the system to escape from a local minimum depends on the properties of the environment in which this minimum is situated. Specifically, it will be dependent on the relative difference between the energy in the current minimum and the energy barriers surrounding it compared to the forcing.

To obtain further insights into the observed behavior of the mean energy, we study a simple model of energy landscape dynamics. Rather than model the dynamics during the entire shearing cycle, we chose to model the change in energy after a cycle. To simplify the model, the position of the particle, representing the vector of coordinates of the system, is constrained to a square lattice with linear size N. Each lattice site has a potential energy chosen from a multivaried Normal distribution with a correlation length σ:

$$P[(u(\mathbf{r}_1), u(\mathbf{r}_2), ..., u(\mathbf{r}_N))] = \frac{1}{(2\pi)^{N/2}|\Sigma|} e^{\sum_{k,m}^{N} u(\mathbf{r}_k)\Sigma_{km}^{-1}u(\mathbf{r}_m)}, \tag{5}$$

where the $\mathbf{r}_k$ is a position of a lattice site,

$$\Sigma_{km} = C[u(\mathbf{r}_k), u(\mathbf{r}_m)] = e^{-\frac{|\mathbf{r}_k - \mathbf{r}_m|^2}{\sigma^2}}, \tag{6}$$

is the covariance matrix and $C[u(\mathbf{r}_i), u(\mathbf{r}_j)]$ is the covariance function. Each point on the lattice represents a local minimum of the potential energy and the correlation length σ represents correlations between minima that are close-by in configuration space.

To capture the combined effects of lowering energy barriers during a shearing cycle, the randomness of the energy landscape and the randomness of the displacement, we suggest a model of dynamics on a lattice in which each step includes a random step from the current lattice site to a neighboring site. However, such a step is allowed only when the energy of the neighboring site after subtracting the forcing energy f is lower than the energy of the current site:

$$u_k(f) = u_k(0) - f \leqslant u_i(0). \tag{7}$$

Here $u_i(0)$ is the unperturbed energy of the site i in which the system is positioned before the shearing cycle, and $u_k(0)$ is the unperturbed energy of site $k \in \mathcal{N}(i)$ where $\mathcal{N}(i)$ is the set of nearest neighbors of site i. For an illustration on a two-dimensional lattice, see Fig. 5.

If the condition Eq. (7) is not met, then the algorithms waits for the next time-step. The forcing parameter f represents the energy lowering effect of the maximal forcing applied during a shearing cycle. This effect is due to the change in potential energy when the system is subject to a maximal strain amplitude $\gamma_{\max}$:

$$u_k(\gamma_{\max}) = u_k(0) - \sigma_{\max}\gamma_{\max} \approx u_k(0) - \mu\gamma_{\max}^2, \tag{8}$$

where $\gamma_{\max}$ is the maximal strain amplitude in the particle simulation or experiment and $\sigma_{\max}$ is the corresponding maximal stress. From elasticity theory $\sigma_{\max} = \mu\gamma_{\max}$ where μ is the shear modulus which we are assuming is approximately

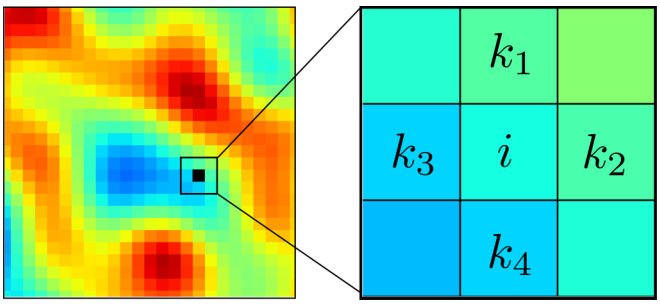

FIG. 5. A close-up of a two-dimensional energy surface used in the model, showing the lattice scale with respect to the typical gradients in potential energy values. A further close-up (right) shows the energy at position i and its neighboring positions $k_j \in \mathcal{N}(i)$. The value of the potential energy increases with color from cold to warm. Note that the scale at which the energy changes is larger than the scale of a lattice site and is related to the correlation length σ.

constant (in practice μ typically changes somewhat due to rearrangement of particles, an effect which will not be taken into account here). From this equation we see a simple relation between f and $\gamma_{\max}$:

$$f = u_k(\gamma_{\max}) - u_k(0) \approx \mu\gamma_{\max}^2. \tag{9}$$

This suggests that

$$\gamma_{\max} \propto \sqrt{f}, \tag{10}$$

which will be assumed in the following. The dynamics is illustrated in Fig. 5. While we believe that the model captures some aspects of the dynamics, due to our simplifying assumptions, there are several features that are not captured. First, the dynamics in the model is isotropic in the energy landscape, which is not the case in a sheared amorphous solid since in those systems the external forcing is applied in a certain direction. Second, we assume that the energy barriers are due to the energy difference between positions i and k which should not be strictly true in an amorphous solid since the system encounters larger energy barriers during the shearing cycle. Another feature that is not captured in the simple model is the fact that under AQS conditions the dynamics is deterministic. For this reason, for small forcing, the dynamics will be confined to a compact region in the energy landscape, similarly to the dynamics in an amorphous solid [24] but will not be repetitive since the randomness is encoded in the dynamics—at each time step it reaches a new point contrary to the dynamics in the particle simulations which enters a limit cycle where the system is visiting the same point over and over after each cycle. Below we describe simulations based on these principles and their results.

A. Model results

Due to memory and simulation time constraints we only simulated the dynamics on two- and three-dimensional surfaces which is to be contrasted with the much larger number of degrees of freedom in a particle simulation of amorphous solids (in the simulations discussed here, the number of degrees of freedom, or dimension of the vector of coordinates $\mathbf{r}_n$ was $2N = 32\,768$). Nevertheless, even for such a small number of dimensions, we observed dynamics that is qualitatively similar to the dynamics observed in particle simulations. For the two-dimensional energy landscape we ran the simulations for forcing values in the range $F \in [0, 3]$. The forcing was normalized such that it is effectively a percentage of the difference between the energy of the maximum and minimum energy of each surface:

$$f = F\frac{(E_{\max} - E_{\min})}{100}. \tag{11}$$

In the two-dimensional simulations we used lattices of dimensions 1000×1000 and in the three-dimensional simulations we used lattices of dimensions $500 \times 500 \times 500$. In both cases we used periodic boundary conditions and correlation length $\sigma = 0.1$. For each dimension ($d = 2, 3$) we ran the simulations on 10 different random surfaces, on each one of them we ran 10 000 random walker realizations (1000 in the $3D$ simulations) half of them starting from the global minimum and the other half from the global maximum of the surface (we do not believe that the initial configurations in the particle simulations were close to the global maximum or minimum of the energy but the idea was to use initial conditions that are consistently of high or low energy). We can see in Fig. 6 that similarly to the particle-based simulations,

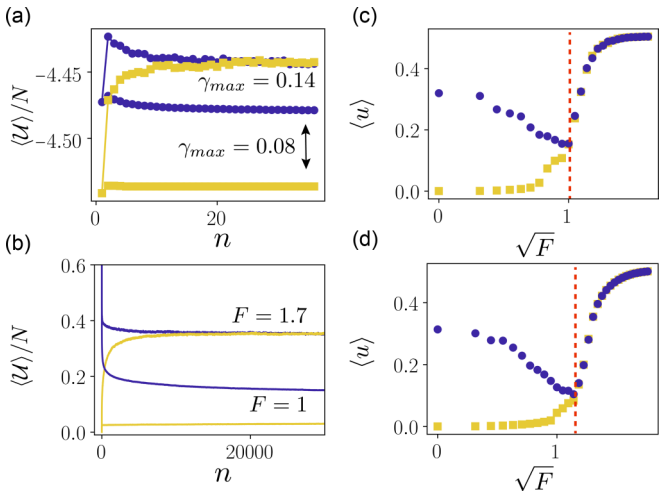

FIG. 6. (a) Transient dynamics observed in the particle simulations starting from a fast quench (blue circles) and a slow quench (yellow squares). For $\gamma_{\max} = 0.08 < \gamma_c$ the lines do not meet, while for $\gamma_{\max} = 0.14 > \gamma_c$ the different initial conditions reach the same steady state. (b) Transient dynamics observed in the model (three-dimensional surface) starting from the minimum (yellow lines) and maximum (blue lines) of the energy landscape. For $F = 1 < F_c$ the lines do not meet, while for $F = 1.7 > F_c$ the different initial conditions reach the same steady state similarly to the behavior observed in (A). In both simulations and model the steady state is ergodic for $\gamma_{\max} > \gamma_c$ ($F > F_c$) and nonergodic for $\gamma_{\max} < \gamma_c$ ($F < F_c$). (c) Average energy using the energy landscape model starting from the minimum (yellow squares) and maximum (blue circles) of the energy landscape for different forcing parameters for simulations on a two-dimensional surface. (d) Same simulations on a three-dimensional energy surface. In both cases, the observed behavior is qualitatively similar to the one shown in Fig. 2. Dotted, vertical, red lines mark $\sqrt{F_c}$.

for forcing values smaller than a critical value $F < F_c$, starting from the two different regions in the energy landscape, the system reaches two different asymptotic values of the average energy and for forcing values F_c or larger ($F_c \approx 1$ for the 2D system and $F_c \approx 1.2$ for the 3D system at the simulated system sizes), different initial conditions end in the same average energy values after a transient [see comparison of the transient behavior between the particle simulations and model in Figs. 6(a) and 6(b)]. This is an indication that the system becomes ergodic for $F > F_c$, in the sense that the energy is independent on the initial conditions. To understand the dynamics microscopically, we can look at simulation movies in the Supplemental Material [26]. We can see there that for $F < F_c$ the dynamics is trapped in a local region while for $F > F_c$ it is free to explore large parts of the energy landscape (see Supplemental Material [26] for movies of the dynamics at $F < F_c$ and $F > F_c$.

In Figs. 6(c) and 6(d) we can see that on both two- and three-dimensional hyper-surfaces, for initial conditions at the minimum, the energy keeps increasing with the forcing, while for initial conditions at the maximum, the energy decreases as long as the forcing is smaller than F_c. For small initial energy, the forcing causes only a moderate increase in the potential energy since the size of the volume that is accessible to the system due to the forcing increases gradually. For a large initial energy, the decrease in the mean energy is much steeper since a small increase in F opens up larger regions with significantly lower energies. When the forcing is larger than F_c, the average energy at the steady state keeps increasing. All of these features are in qualitative agreement with the results obtained from the particle simulations even though the dynamics in the model is much simpler and we have further made the simplifying assumption that the energy surface is Gaussian and two- or three-dimensional.

B. Diffusive behavior

To further understand the ergodic behavior of the system, we study the mean-square displacement (MSD) which provides an indication of the size of the region on the landscape that is being explored. We performed simulations on a 2D 500×500 lattice and averaged over 1000 random wakers starting from the minimum and maximum of 10 random surfaces with $\sigma = 0.1$. As we can see in Fig. 7, the dynamics is qualitatively similar to the dynamics that was observed in particle simulations of amorphous solids [13]—for small values of F the MSD reaches a plateau, while for large enough F, the dynamics is diffusive. For values of F close to but above $F_c \approx 1.8$ (F_c here is larger than in the energy simulations due to the smaller system size used) the diffusion coefficient increases gradually and starting from $F = 5$ the behavior is simple diffusion with a constant diffusion coefficient. We also observe transient super-diffusion which is consistent with observations in particle simulations [13]. The transition from an asymptotically constant MSD to a diffusive MSD ($\langle r^2 \rangle \sim t$) is a clear indication of a transition from nonergodic to ergodic behavior. One difference between the model and particle simulations is that since the system does not reach a limit-cycle, it takes the MSD longer time to reach a plateau and this sometimes occurs after the energy settled into a constant value.

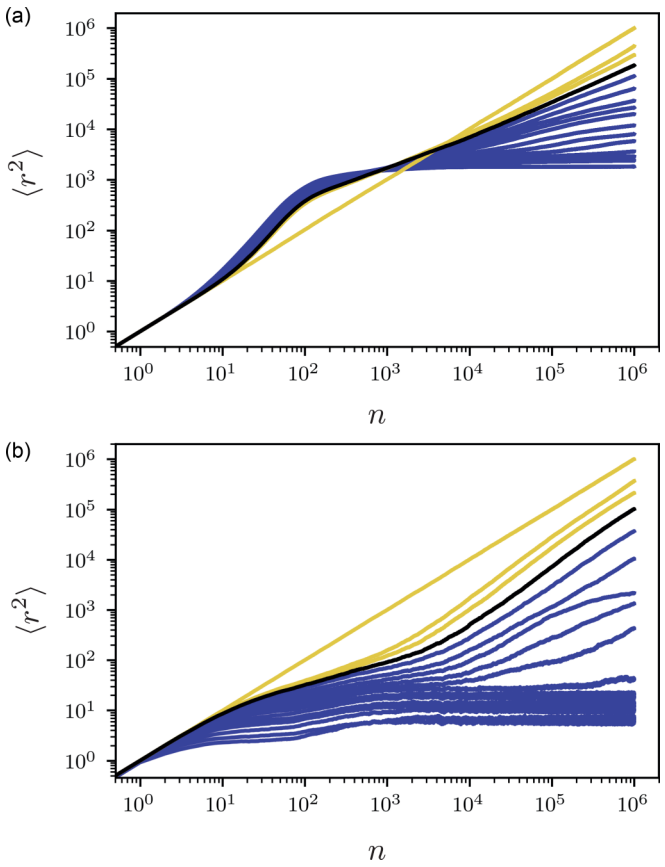

FIG. 7. (a) Mean-square displacement in a two-dimensional model subject to different forcing $F = 0.5, 0.6, 0.7, 0.8, 0.9, 1.0, 1.1, 1.2, 1.3, 1.4, 1.5, 1.6, 1.7, 1.8, 1.9, 2.0, 5.0$, starting from the maximum of the energy landscape. (b) Mean-square displacement for the same forcing values as in (a) starting from the minimum of the energy landscape. In both cases blue curves represent dynamics with $F < F_c$ while the yellow curves represent dynamics for $F > F_c$. The black curve represents the dynamics at $F_c \sim 1.8$. For $F > 5$ the MSD does not change with F and appears as a straight line (simple diffusion).

C. Ergodic behavior of the mean energy

One of the pronounced features of the average potential energy in the particle simulations, is that for an initial configuration prepared with a fast quench, such that its initial potential energy is high, upon increasing the maximal strain amplitude (but keeping it below the critical value γ_c), the steady-state values of the energy decrease. However, for maximal strain amplitudes above the critical value, the steady-state energy increases. This effect is reproduced by the energy surface model which also provides a simple explanation for this observation (Fig. 8). For initial conditions at the maximum of the energy landscape, any change in the position on the energy landscape results, on average, in a downhill motion on the energy surface and thus causes the mean energy to decrease. However, increasing the forcing parameter also allows the system to explore areas of larger and larger energies. These two

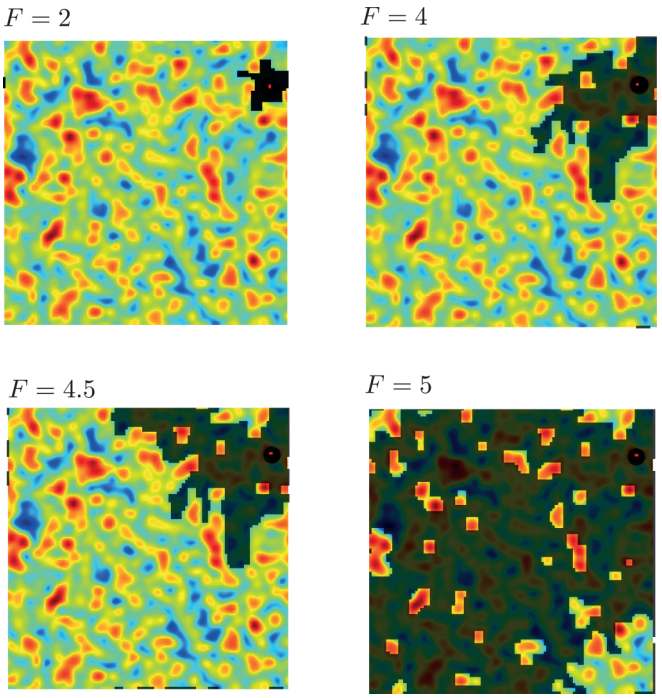

FIG. 8. Parts of the energy landscape covered by a single random-walker starting at the maximum of the landscape for different forcing parameters ($F = 2.0, 4.0, 4.5, 5.0$) for a two-dimensional 100×100 system.

competing tendencies meet close to the critical point leading to the observed cross-over behavior (see Fig. 9 for illustration). The increase of the mean potential energy for $F > F_c$ ($\gamma_{\max} > \gamma_c$) is a feature that cannot be reproduced by a one-dimensional energy landscape model, of the sort that is commonly used in theories of plasticity of amorphous solids [27–29] and is a result of the fact that even when the system becomes ergodic in the sense that different initial conditions lead, on average, to the same steady-state potential energy, there are parts of the landscape that are inaccessible for values of F close to F_c. These parts become accessible as F is increased, causing an increase in the average potential energy.

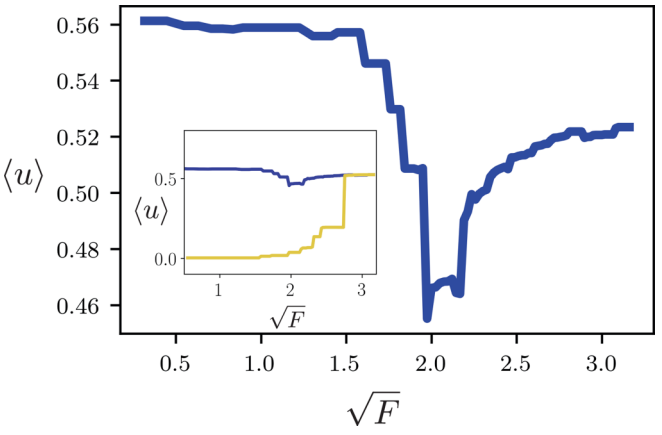

FIG. 9. Average energy of the accessible part of the surface as a function of the forcing parameter for a system starting at the maximum of the energy surface. Since the system is rather small (100×100) the point of transition occurs at a larger value of F than in the systems used in the simulations and can fluctuate significantly from sample to sample. Inset: same results for systems starting both at the vicinity of the maximum (blue) and minimum (yellow) of the energy surface.

IV. DISCUSSION

We have shown, using a model of a two-dimensional amorphous solid, that under athermal quasistatic oscillatory shear, with subyield maximal strain amplitudes, the zero-strain potential energy of an amorphous solid exhibits both annealing (a decrease in the energy) and rejuvenation (an increase in the energy) depending on the preparation protocol of the initial configuration. This has implications for the rheology of glasses, as well as toward understanding the irreversibility transition. We explain the observed dynamics by studying a simple model of dynamics on a rough energy landscape and show that the model can reproduce qualitatively important aspects of the dynamics observed in our two-dimensional particle simulations. These results indicate that certain features of the irreversibility transition can be understood as resulting from changes in the dynamically accessible regions of the energy landscape when an external forcing is applied. Future studies will focus on studying the behavior of the mean energy and the irreversibility transition in more models in two and three dimension as well as further exploring the effects of using different cooling protocols such as the advanced Monte Carlo methods recently used to show a transition from brittle to ductile behavior in amorphous solids under unidirectional shear [30].

ACKNOWLEDGMENTS

I.R. thanks G. Bel, Y. Ashkenazy, A. Szulc, and M. Mungan for useful discussions. I.R. was supported by the Israel Science Foundation through Grant No. 1301/17.

APPENDIX: SIMULATION DETAILS

1. Simulation details

The interaction potential that we are using is

$$U(r) = \begin{cases} \epsilon\left[\left(\frac{a}{r}\right)^{12} - \left(\frac{a}{r}\right)^{6} + \frac{1}{4} - h_0\right], & \frac{r}{a} \leqslant x_0, \\ \epsilon h_0 P\left(\frac{\frac{r}{a} - x_0}{x_c}\right), & x_0 < \frac{r}{a} \leqslant (x_0 + x_c), \\ 0, & r > a(x_0 + x_c), \end{cases} \tag{A1}$$

which was developed in Ref. [31] and consists of the repulsive part of the standard Lennard-Jones potential, connected via a hump to a region that is smoothed continuously to zero (see Fig. 10). The point x_0 is the position at which the Lennard-Jones potential is minimal, $x_0 = 2^{1/6}$, $x_c = 0.5$, and the position where the potential vanishes is $a(x_0 + x_c)$. The parameter h_0 determines the depth of the minimum. The polynomial $P(x)$ is chosen as

$$P(x) = \sum_{i=0}^{6} A_i x^i, \tag{A2}$$

with the coefficients given in Table I.

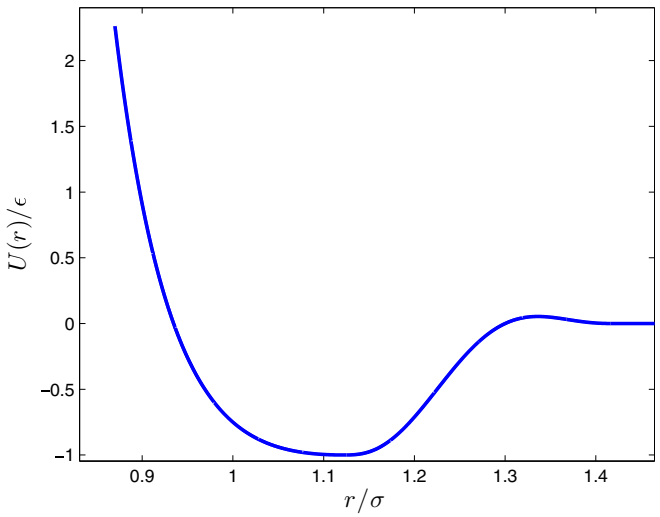

FIG. 10. The radially symmetric potential used in the particle simulations reported in the paper.

2. Units used in particle simulations

We used the reduced simulation units for positing r^*, time t^*, and temperature T^*:

$$r^* = \frac{r}{a}, \tag{A3}$$

$$t^* = \frac{t}{\tau} = t\sqrt{\frac{\epsilon}{ma^2}}, \tag{A4}$$

$$T^* = \frac{k_B T}{\epsilon}. \tag{A5}$$

where $\tau = \sqrt{\frac{\epsilon}{ma^2}}$.

3. Quenching protocol for particle simulations

a. Fast quench

Initial configurations which were referred to as prepared using a fast quench were equilibrated using a standard molecular dynamics algorithm with a Berendsen thermostat for 20τ in $T^* = 1$. Then they were equilibrated at $T^* = 0.1$ for another 50τ and then quenched using the FIRE minimization algorithm to zero temperature.

b. Slow quench

Initial configurations which were referred to as prepared using a slow quench were equilibrated for 10τ at $T^* = 1$ and then cooled down by steps of $T^* = 0.025$ to $T^* = 0.1$ while equilibrating for 10τ after each cooling step. After the last step of equilibrating at $T^* = 0.1$ the system was quenched using the FIRE minimization algorithm to zero temperature.

TABLE I. The coefficients in Eq. (A2).

A_0	−1.0
A_1	0
A_2	1.785826183464224
A_3	28.757894970278530
A_4	−81.988642011620980
A_5	76.560294378549440
A_6	−24.115373520671220

[1] P. G. Debenedetti and F. H. Stillinger, Nature **410**, 259 (2001).
[2] A. Cavagna, Phys. Rep. **476**, 51 (2009).
[3] L. Berthier and G. Biroli, Rev. Mod. Phys. **83**, 587 (2011).
[4] M. Goldstein, J. Chem. Phys. **51**, 3728 (1969).
[5] C. E. Maloney and A. Lemaître, Phys. Rev. E **74**, 016118 (2006).
[6] S. Karmakar, A. Lemaître, E. Lerner, and I. Procaccia, Phys. Rev. Lett. **104**, 215502 (2010).
[7] I. Regev, T. Lookman, and C. Reichhardt, Phys. Rev. E **88**, 062401 (2013).
[8] I. Regev, J. Weber, C. Reichhardt, K. A. Dahmen, and T. Lookman, Nat. Commun. **6**, (2015).
[9] N. C. Keim and P. E. Arratia, Soft Matter **9**, 6222 (2013).
[10] S. Slotterback, M. Mailman, K. Ronaszegi, M. van Hecke, M. Girvan, and W. Losert, Phys. Rev. E **85**, 021309 (2012).
[11] K. Hima Nagamanasa, S. Gokhale, A. K. Sood, and R. Ganapathy, Phys. Rev. E **89**, 062308 (2014).
[12] T. Kawasaki and L. Berthier, Phys. Rev. E **94**, 022615 (2016).
[13] D. Fiocco, G. Foffi, and S. Sastry, Phys. Rev. E **88**, 020301(R) (2013).
[14] N. V. Priezjev, Phys. Rev. E **93**, 013001 (2016).
[15] J. C. Pfeifer, T. Bischoff, G. Ehlers, and B. Eckhardt, Phys. Rev. E **92**, 062208 (2015).
[16] P. Leishangthem, A. D. Parmar, and S. Sastry, Nat. Commun. **8**, 14653 (2017).
[17] N. V. Priezjev, Phys. Rev. E **95**, 023002 (2017).
[18] S. Mukherji, N. Kandula, A. K. Sood, and R. Ganapathy, Phys. Rev. Lett. **122**, 158001 (2019).
[19] J. L. Miller, Phys. Today **72**(6), 16 (2019).
[20] A. D. S. Parmar, S. Kumar, and S. Sastry, Phys. Rev. X **9**, 021018 (2019).
[21] P. Das, A. D. Parmar, and S. Sastry, arXiv:1805.12476.
[22] D. J. Lacks and M. J. Osborne, Phys. Rev. Lett. **93**, 255501 (2004).
[23] L. Boué, H. G. E. Hentschel, I. Procaccia, I. Regev, and J. Zylberg, Phys. Rev. B **81**, 100201(R) (2010).
[24] I. Regev and T. Lookman, J. Phys.: Condens. Matter **31**, 045101 (2018).
[25] E. Bitzek, P. Koskinen, F. Gähler, M. Moseler, and P. Gumbsch, Phys. Rev. Lett. **97**, 170201 (2006).
[26] See Supplemental Material at http://link.aps.org/supplemental/10.1103/PhysRevE.101.012603 for simulation movies.
[27] P. Sollich, Phys. Rev. E **58**, 738 (1998).
[28] P. Sollich, F. Lequeux, P. Hébraud, and M. E. Cates, Phys. Rev. Lett. **78**, 2020 (1997).
[29] M. L. Falk and J. S. Langer, Phys. Rev. E **57**, 7192 (1998).
[30] M. Ozawa, L. Berthier, G. Biroli, A. Rosso, and G. Tarjus, Proc. Natl. Acad. Sci. USA **115**, 6656 (2018).
[31] E. Lerner and I. Procaccia, Phys. Rev. E **79**, 066109 (2009).